NASA Technical Paper 2884

1988

Cyclic Loads Tests of Carbon Involute Solid Rocket Motor Outer Boot Ring Segments

Rafiq Ahmed
George C. Marshall Space Flight Center
Marshall Space Flight Center, Alabama

National Aeronautics and Space Administration

Scientific and Technical Information Division

TABLE OF CONTENTS

LIST OF ILLUSTRATIONS

LIST OF TABLES

TECHNICAL PAPER

CYCLIC LOADS TESTS OF CARBON INVOLUTE SOLID ROCKET MOTOR OUTER BOOT RING SEGMENTS

I. INTRODUCTION

On December 23, 1987, a Solid Rocket Motor (SRM) nozzle Outer Boot Ring (OBR) failed at the end of the Development Motor 9 (DM-9) test firing in Utah. This ring was constructed of carbon cloth phenolic (CCP) composite material laid in an involute arrangement. As a result, NASA selected the structural backup ring used in DM-8 to commence shuttle flights after the 1986 Challenger disaster. In an effort to explain the boot ring failure, a series of structural tests and analyses were devised for the DM-9 configuration ring. Among these was a series of cyclic loads tests of OBR segments.

A. Purpose

The immediate objective of the cyclic loads tests was to assess the cumulative damage, if any, from the cyclic loading incurred by gimballing the SRM nozzle during the DM-9 firing. To do this, six 30-in. segments were cut from an involute ring and instrumented with strain gages and EDIs. Three specimens were loaded directly to failure without cycling, and the other three were loaded to failure after being cyclically loaded to simulate the DM-9 nozzle thrust vector control (TVC) duty cycle.

B. Summary

This report discusses the cyclic load tests and presents the recorded data. The results of the individual specimens are compared with each other and with the analytical model, and an assessment of the extent of cumulative damage from cycling is given.

The series of cyclic loads tests on the SRM involute OBR was conducted in the period of March 14 to March 25, 1988. Strain gages and EDIs were placed at various locations on each sgement with load, strains, and displacements recorded for each specimen tested (Figs. 1, 2, and 3).

II. CYCLIC LOADS TEST

The series of cyclic loads tests was conducted under the supervision of Mr. David Snoddy (ET52).

A. Test Specimens

Each of the six specimens was a 30-in. nominal circumferential-length segment of the involute OBR. The segments had an inner radius of 48.685 in., an outer radius of 50.385 in., a width of 6.5 in., and a thickness of 1.7 in. The moment of inertia about the in-plane axis of the beam cross section is 2.66 $in.^4$ with a section of modulus of 3.129 $in.^3$.

B. Test Fixture

The test fixture consisted of a 50,000-lb load cell with a hydraulic actuator and all the appropriate hardware needed to load the specimen in four-point bending. A 20,000-lb load cell was used for Test No. 1 but was found to be inadequate to break the specimen. Tests 1A through 6 were conducted with a 50,000-lb load cell.

The specimen was mounted with fixtures spaced 24-in. apart and configured such that it could move in its longitudinal direction.

Essential to this test was the proper application of the four-point bending loads to the segment. This was accomplished by using Teflon pads to distribute the load and minimize friction between load applicator and segment. A load point was applied 6-in. from each mounting fixture (Fig. 1).

C. Instrumentation

Each segment was instrumented by the Test Laboratory (ET52) at MSFC with uniaxial and triaxial strain gages. All gages were placed at various positions in the middle of each specimen (Fig. 3). The uniaxial gages measured tensile and compressive outer fiber strains as well as strains across the thickness. The triaxial gages measured strains in the outer fiber and cross-width directions. A total of 12 channels were recorded per segment tested.

D. Procedure

Load was applied by a single actuator located at the mid-point of the 30-in. segment and distributed to two loading pads, producing four-point bending. Three specimens (Test Nos. 1, 2, and 3) were loaded to failure without cycling, and the final three specimens (Test Nos. 4, 5, and 6) were cycled 40 times and then loaded to failure. Test No. 4 was given a sinewave cycling from 4400 lb (approximately 1100 microstrain) to 6000 lb (approximately 1500 microstrain), simulating the DM-9 nozzle gimballing loads. Test Nos. 5 and 6 were subjected to double the above loads (8800 to 12,000 lb) when it was seen that the Test No. 4 failure load was not significantly different from the failure loads of Test Nos. 1A, 2A, and 3. All cycled specimens were loaded to failure after their respective cyclic loadings. Loads, deflections, and strains were recorded during all cyclic and failure loadings. All tests were conducted at room temperature (approximately 70°F).

It is important to note that two anomalies occurred in these tests. First, Test No. 1 was loaded to 16,000 lb and then unloaded when test personnel realized (from the low strain readings) that the specimen would not fail at the 20,000-lb capacity of the original load cell. The load cell was changed to

50,000 lb and the specimen loaded to failure in Test No. 1A. Second, specimen No. 2 slipped out of the test fixture during Test No. 2 as the load approached 34,000 lb (which was well above Test No. 1A's failure load). Corrective action was taken for Test No. 2A (and also to prevent slippage on the subsequent tests) and the specimen failed at approximately 31,000 lb.

E. Results

The deflections and strains at maximum load are shown in Table 1. Load versus deflection and load versus strain plots are given in Figures 5 through 20. Almost all plots showed nonlinearity, indicating plasticity in the material.

III. ANALYTICAL MODEL OF TEST

A simple beam analysis was made to give a mathematical prediction of the failure load. Strains were assumed to vary linearly (as a function of distance in the thickness direction) on both the tension and compression sides of the neutral axis; however, the neutral axis does not lie in the middle of the cross section since the tension stress-strain curve is bilinear and the compression stress-strain curve is linear. The analysis is detailed in the Appendix. The ultimate load required by the actuator was predicted to be 21,400 lb. Since the radius of curvature is sufficiently large (the radius of the boot ring is much greater than five times the thickness), each curved segment can be approximated as a straight beam.

IV. DISCUSSION

A. Failure Loads

This section compares the cycled specimen failure loads with the uncycled specimen failure loads. Comparisons with the analytical values are also made. No significant change in ultimate load was incurred by any of the cycled specimens (as compared to the uncycled specimens) from either of the two cyclic load spectrums. As shown in Table 1, the loads required for failure of the cycled specimens are slightly higher than those for the uncycled specimens. There are three possible reasons for this:

1) Test Nos. 1 and 2 experienced anomalies which required their specimens to be run twice at substantial (over 50 percent of failure) loads, thus giving lower failure loads due to decreased fracture toughness.

2) Some strain hardening may have occurred during cycling without significantly reducing the fracture toughness of the material.

3) There exists data scatter among the tests.

B. Load Versus Strain and Deflection

Typically, most of the load versus deflection and load versus strain curves were linear in the elastic range with a decrease in slope as higher loads were reached. However, an interesting phenomenon occurred in Test No. 2A, where an increase in slope of both the load versus deflection and load versus strain curves was noted as the load approached ultimate. These plots also showed that the specimen stiffness was lower in the linear range for Test No. 2A than for Test No. 2. This was attributed to matrix degradation in the CCP that resulted from the first loading of 34,000 lb (which was at or near imminent failure), while the increase in stiffness at the higher load levels of Test No. 2A was attributed to microcracking of the fibers (this most likely happened in Test No. 2). The fibers sustain most of the load at these higher load levels. It is interesting to note that none of the cyclic loadings produced a similar effect in the material, since they were of insufficient peak load.

C. Elastic and Plastic Moduli

To analyze the elastic moduli, the load versus strain data were converted to outer surface stress versus surface strain. This was accomplished by using the beam stress relation,

$$\sigma = MC/I$$

for a beam of rectangular cross section ($I = 0.0833 \times b \times h^3$). The curvature of the boot ring segment was small enough to be neglected. The resulting stress strain data for each test were then reduced by linear regression to give an elastic modulus and plastic modulus for a bilinear hardening curve. Values for these are listed in Table 2.

The agreement between the elastic moduli of the different samples is quite good; the scatter between the lowest and the highest moduli (not including Test No. 2A) is only 12 percent. As noted previously, Test No. 2A's modulus is low due to degradation of the part from Test No. 2. The increase in Test No. 2A's plastic modulus is clearly seen.

A substantial (300 percent) difference between the moduli of these tests and those established in small-specimen "coupon" tests (run at the Southern Research Institute) was noted. A four-point bending test closely approximates uniaxial tension at the outer fiber, and should therefore yield a modulus close to that obtained from a tension test. Even if the OBR segment is assumed to be a wide beam, the modulus will increase by less than 10 percent for a Poisson's ratio of 0.3. However, future tests should evaluate the width to thickness ratio effects in bending of these materials.

D. Comparison of Test and Analysis

The averge load required to fail a 30-in. boot ring segment (discounting the anomalous test 1 and test No. 2A) in the series of cyclic loads tests is 32,915 lb, whereas the analysis predicted about 21,436 lb. This deviation was attributed to the difference in material properties between these tests and those

from the small-sample "coupon" tests which were the basis for the analysis. The theory also assumed isotropic material properties when the composite material of the boot ring is in reality anisotropic or orthotropic.

E. Failure Surfaces

Fiber failures and delaminations were noticed in the failures of all specimens. Fiber breakage occurred primarily on the tension side of each specimen except No. 5, while delaminations occurred mostly on the compression side. This happened because the compressive fiber strength of the material is much greater than the tensile strength; therefore, the compressive-side material tended to peel away during failure.

Specimen Nos. 4, 5, and 6 showed significant secondary cracking through the thickness of the segment, apparently caused by the cycling routine imposed on each. The matrix, but not the fibers, seemed to have been degraded by cycling, thereby facilitating crack propagation. The secondary cracking may also account for the unique tension-side delamination in Specimen No. 5.

The failure surfaces of each specimen are shown in Figures 21, 22, and 23.

V. CONCLUSIONS

The most important result obtained from this series of tests is the lack of effect of boot ring thrust vectoring on the strength of the outer boot ring. The tests showed that there is, in fact, a slight increase in ultimate load capacity in the involute construction CCP material after applying a sinewave cycling load with peaks of less than 20 percent of ultimate strength.

The analytical model used to baseline the series of cyclic loads tests gave a conservative estimate of the actual failure load (without cycling). As stated previously, the anisotropy of the carbon cloth phenolic positively affected the actual failure loads. This gives confidence in applying the conventional isotropic theory to analysis of involute carbon phenolic beams (at room temperature) if high conservatism is not a problem.

Several phenomena of interest from an engineering standpoint were observed in the cyclic loads tests. Among these was the discovery of a plastic modulus larger than the elastic modulus in Test No. 2A, as well as the substantial decrease in elastic modulus for Test No. 2A versus Test No. 2. These reflect the unique characteristics of the fiber-matrix mix that makes up most composite materials. Further tests should be performed to explore these phenomena and acquire more experience in testing composite structures, as well as to validate analytical and finite element models that account for composite material anisotropy. Other tests are needed to better establish a material properties database.

APPENDIX

DERIVATION OF FAILURE LOAD FOR OBR 30 INCH SEGMENT IN FOUR POINT BENDING

Looking at the beam, the following stress and strain profiles are exhibited through the thickness:

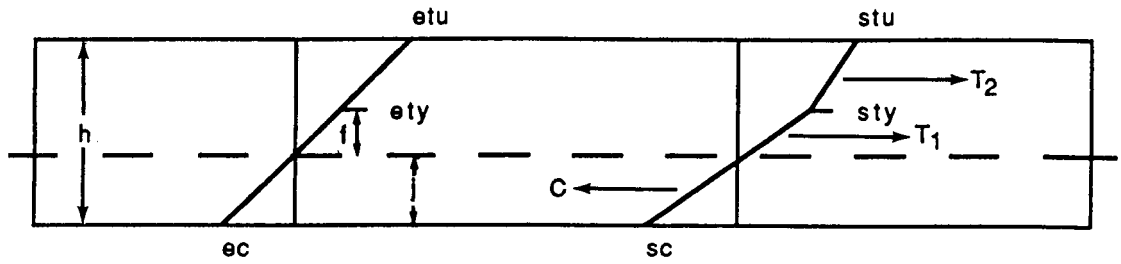

Note that, since the tension stress-strain curve is bilinear and the compression curve is not, the neutral axis shifts toward the compression side of the beam. The beam is assumed to have the same material properties all through its thickness. The following material properties are needed:

s_{tu} = ultimate tensile stress = 16000 psi
s_{ty} = yield tensile stress = 8000 psi
e_{tu} = ultimate tensile strain = 0.012
e_{ty} = yield tensile strain = 0.003
s_{cu} = ultimate compressive stress = 42600 psi
e_{cu} = ultimate compressive strain = 0.0168
h = height = 1.70 in
f = location in beam thickness direction where fibers first start to yield
j = neutral axis location

1.) First, the location of the neutral axis, j, must be found:

Similar triangles:

$$f/e_{ty} = j/e_c = (h-j)/e_{tu}$$

$$f = (e_{ty}/e_{tu})(h - j)$$

Now find forces T1, T2 and C:

$$T1 = (s_{ty}\, f/2) = (s_{ty}\, e_{ty}/2e_{tu})\, (h-j)$$

$$T2 = ((s_{ty} + s_{tu})/2)\, (h - j - f) = ((s_{ty} + s_{tu})/2)\, (h - j)(1 - e_{ty}/e_{tu})$$

$$C = s_c\, j/2 = (e_{tu}\, j/(h - j))\, (s_{cu}/e_{cu})\, j/2$$

When the sum of the forces is set equal to zero, i.e.,

$$T1 + T2 - C = 0$$

the following equation is obtained after appropriate substitutions:

$$17000 - 10000j - (15214.29/(1.7 - j))j^2 = 0$$

After iterative solving, the answer is $j = 0.76$ in.

2.) Now the moments are summed about the neutral axis to find the total moment per inch of beam width:

$$m = -c(j/3) + T1(j + .666f) + T2\, (j + f + (h - j - f)/2)$$

where $f = (e_{ty}/e_{tu})\, (h - j) = 0.235$ in and $h - j - f = 0.705$ in

Substituting, $m = 9894$ lb-in/in

Total moment = $M = mw = m(6.5\text{ in}) = 64310$ lb-in

3.) Now, substituting this into the four-point bending relation:

$$P/2 = M/6\text{ in} = 10718\text{ lb}$$

$$P = 21436\text{ lb}$$

Thus, the predicted failure load is 21436 lb.

TABLE 1. LOAD, DEFLECTION, AND STRAIN READINGS AT MAX. LOAD

(LOAD IN LBS, DEFLECTION IN INCHES, STRAIN IN MICROSTRAIN)

Test #	L1001	D1001	D1002	D1003	S1001	S1002	S1003	S1004	S1005	S1006
*1	16002	0.458	0.02	-0.23	-139	-152	4380	-4124	4188	-4214
1A	29483	0.937	-0.509	-0.014	-672	-760	10584	-8447	9675	-8350
*2	33964	0.853	-0.266	0.000	-556	-805	9645	-8472	10199	-8337
2A	30610	0.653	0.045	-0.433	-493	-662	341	-7652	8971	-7402
3	32740	0.673	-0.291	-0.127	-640	-650	9165	-7407	8090	-7388
^4	33125	0.807	-0.142	-0.326	-577	-647	7741	-8284	-8143	8858
^^5	34590	0.850	-0.14	-0.335	-830	-577	7514	-8037	8505	-8248
^^6	33590	0.861	-0.163	-0.334	-538	-814	9050	-8247	9168	-8297

Test #	1T1001	2T1001	3T1001	1T1002	2T1002	3T1002
*1	4228	1533	-867	-4087	-1746	844
1A	9847	3609	-1572	-8371	-3711	1590
*2	10161	3287	-1548	1559	-3181	-8299
2A	8982	3037	-1418	1420	-2908	-7484
3	-1483	3386	8408	1442	-3185	-7405
^4	7984	3718	-1499	1492	-3535	-7869
^^5	-8737	-3404	1526	9271	4110	-1640
^^6	9765	4851	-1654	1629	-3570	-9116

* - test did not go to failure

^ - loaded to failure after 40 cycles from 4400 lb to 6000 lb

^^ - loaded to failure after 40 cycles from 8800 lb to 12000 lb

TABLE 2. ELASTIC AND PLASTIC MODULI AT OUTER FIBERS

TEST #	ELASTIC MODULUS(Msi)	PLASTIC MODULUS(Msi)	AVG. MODULUS(Msi)
*1	7.209	---------	---------
1A	7.230	3.935	5.462
*2	8.169	4.983	7.192
2A	6.352	6.812	6.472
3	7.736	5.580	7.081
^4	7.909	6.141	7.304
^^5	7.831	6.089	7.194
^^6	7.824	5.822	6.695

* - test did not go to failure

^ - loaded to failure after 40 cycles from 4400 lb to 6000 lb

^^ - loaded to failure after 40 cycles from 8800 lb to 12000 lb

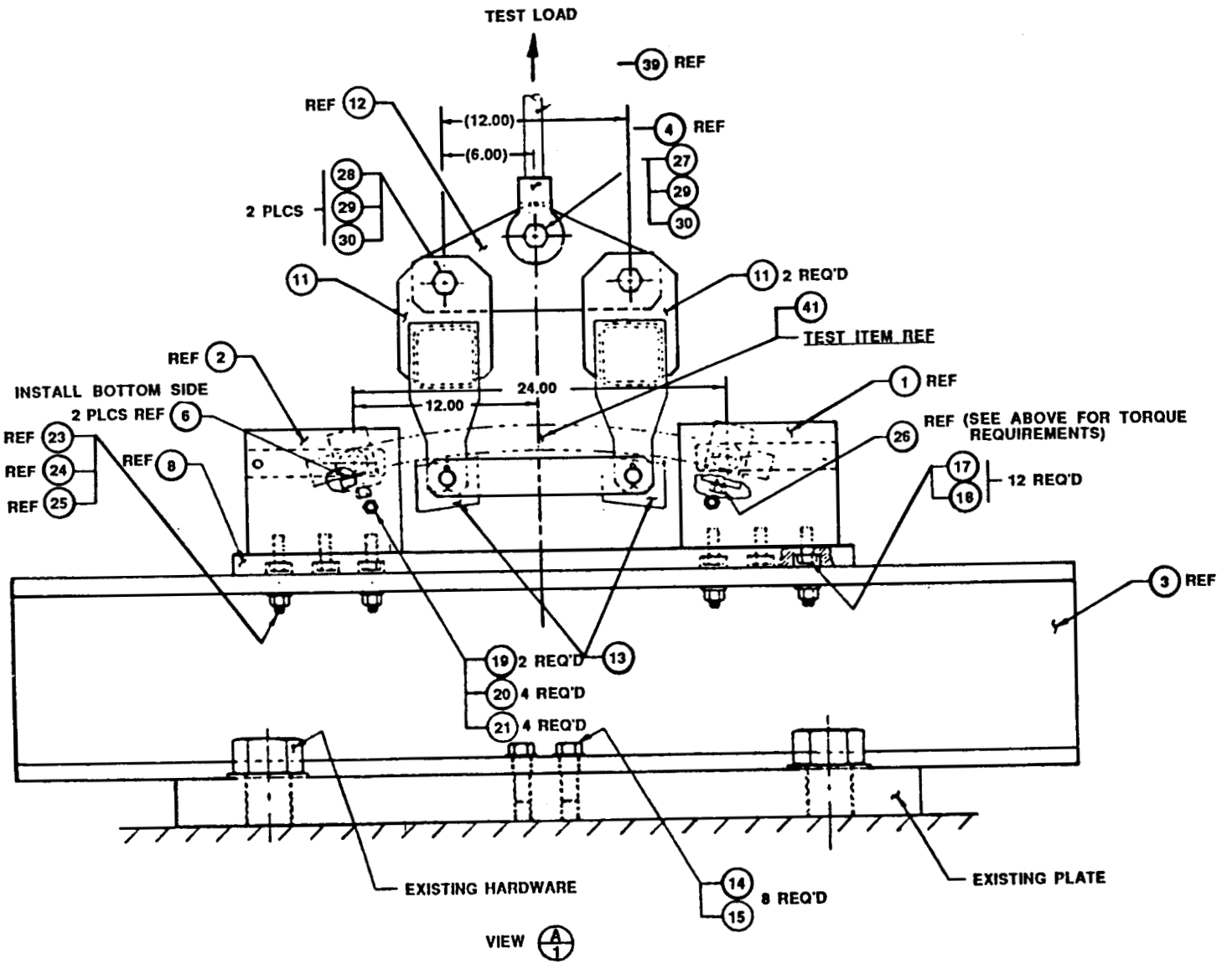

Figure 1. Diagram of test setup.

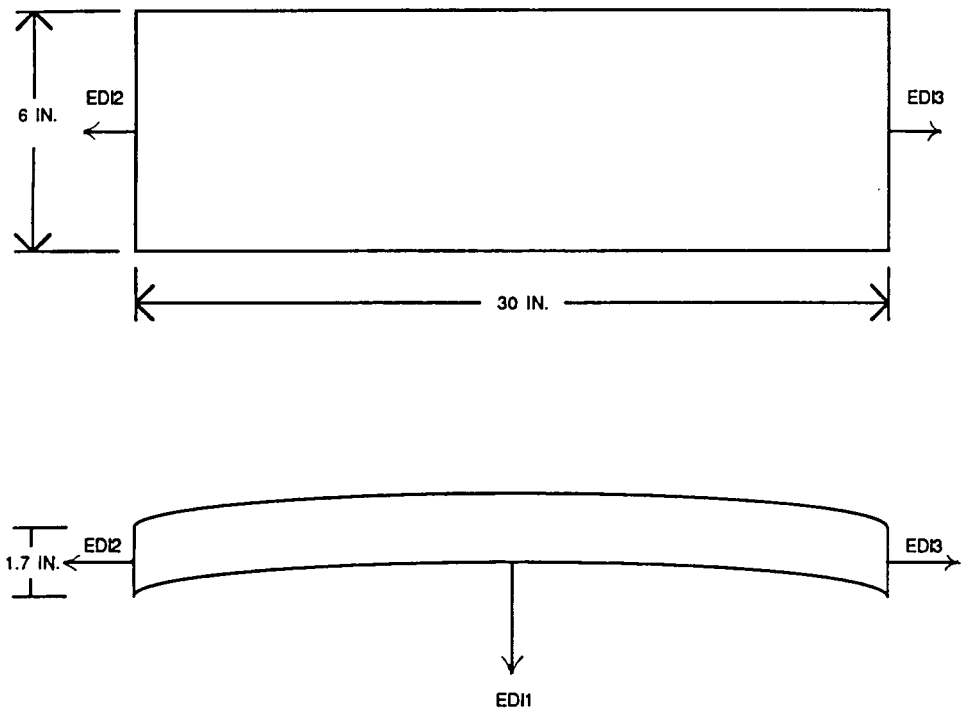

Figure 2. Displacement gage locations for cyclic loads tests.

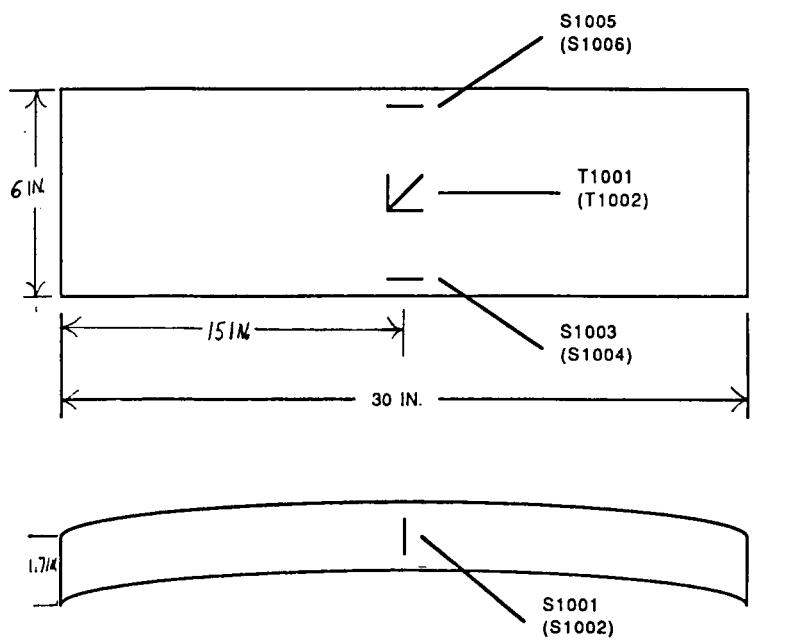

Figure 3. Strain gage locations for cyclic loads tests.

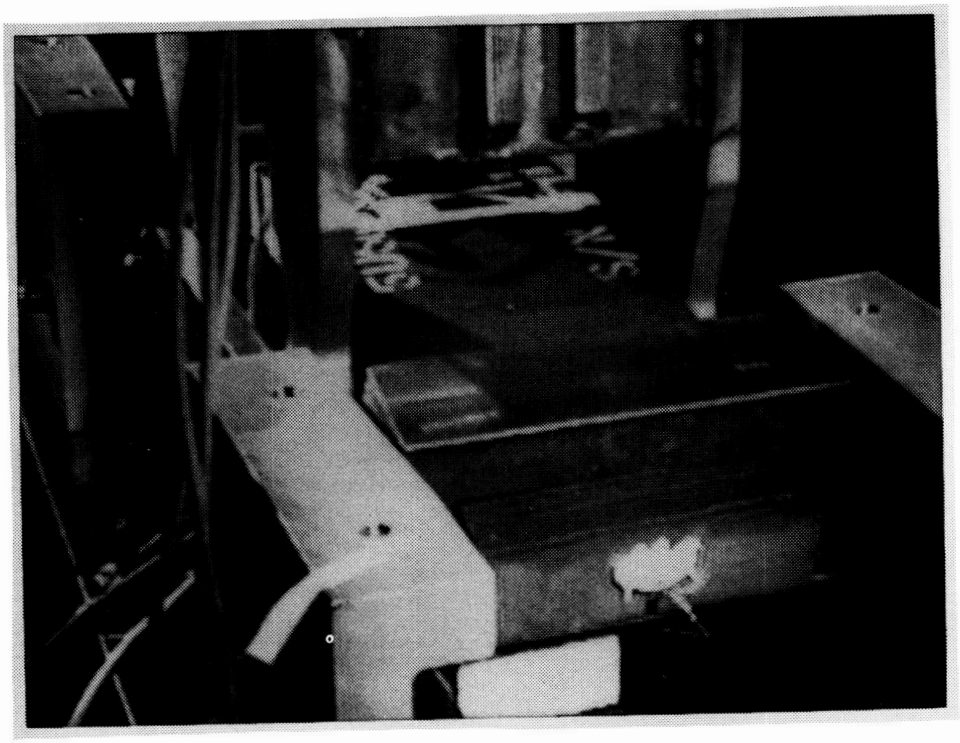

Figure 4. Test setup for cyclic loads tests.

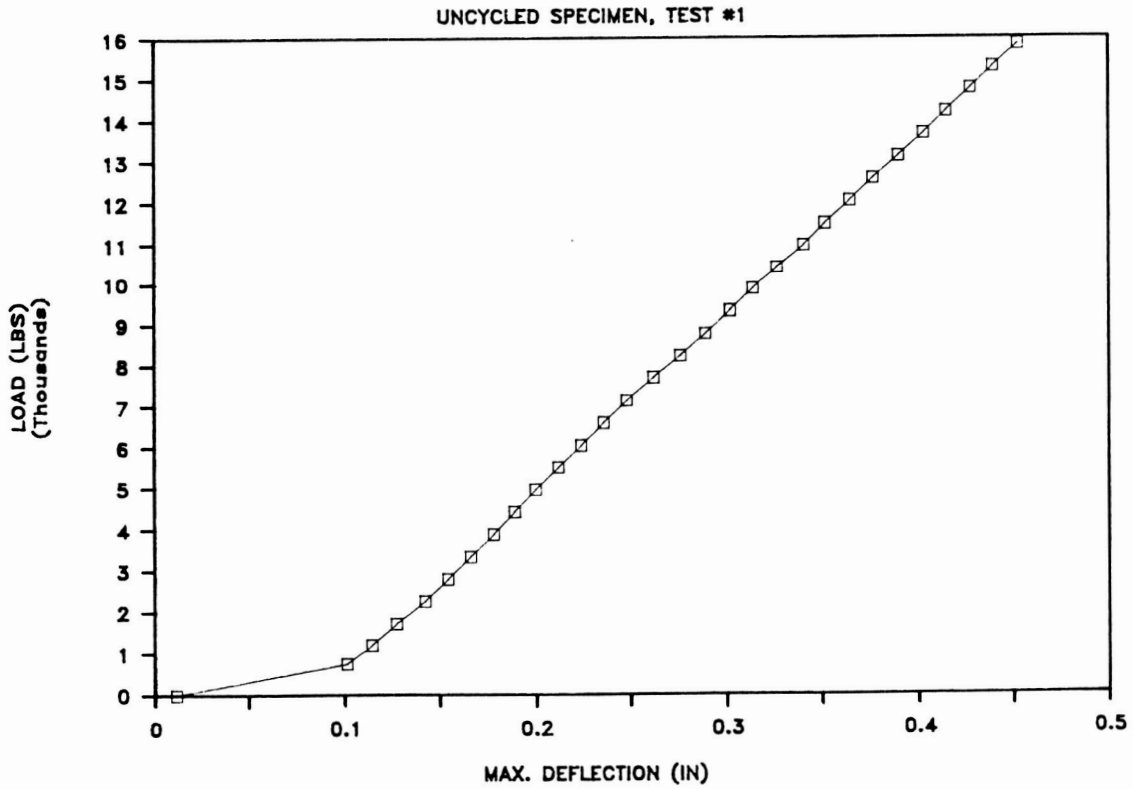

Figure 5. OBR cyclic loads test, uncycled specimen, Test No. 1.

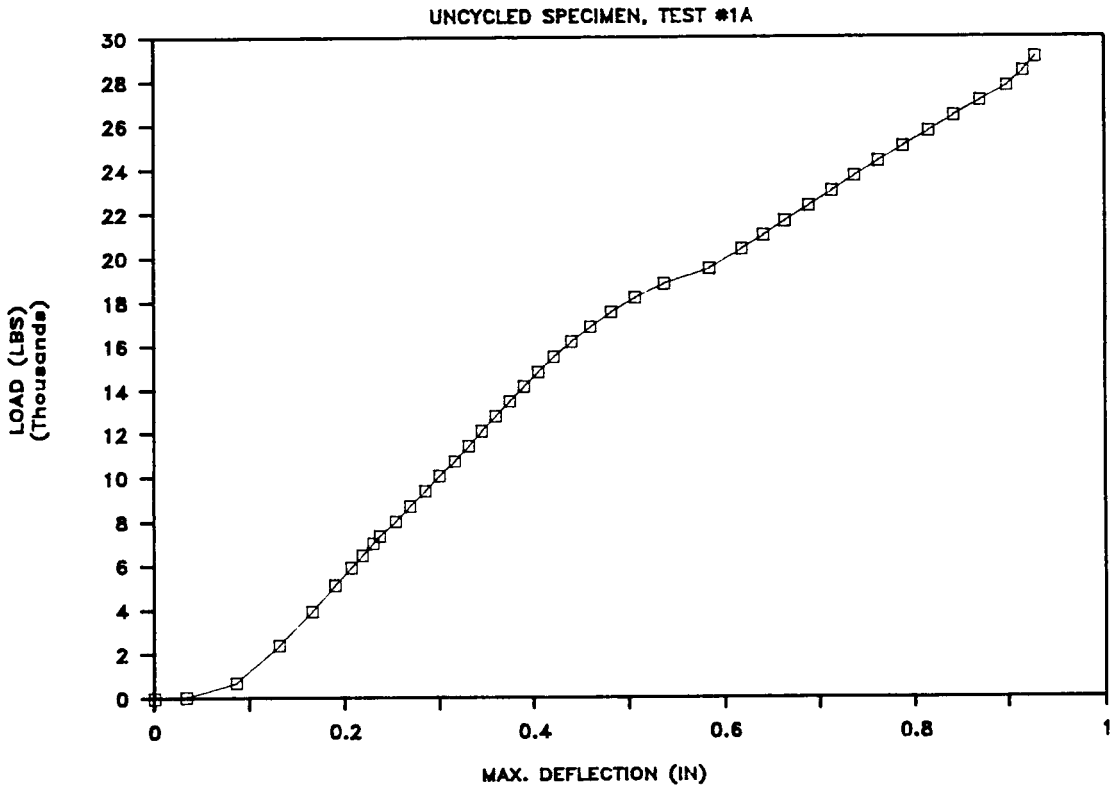

Figure 6. OBR cyclic loads test, uncycled specimen, Test No. 1A.

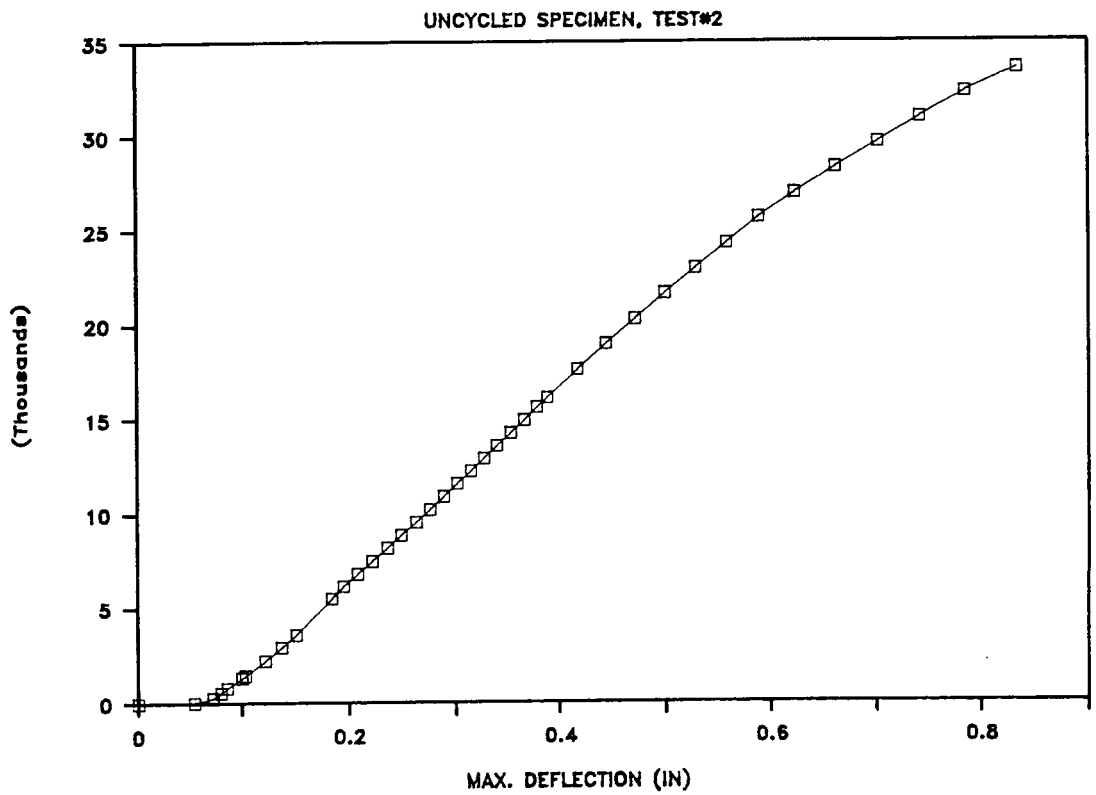

Figure 7. OBR cyclic loads test, uncycled specimen, Test No. 2.

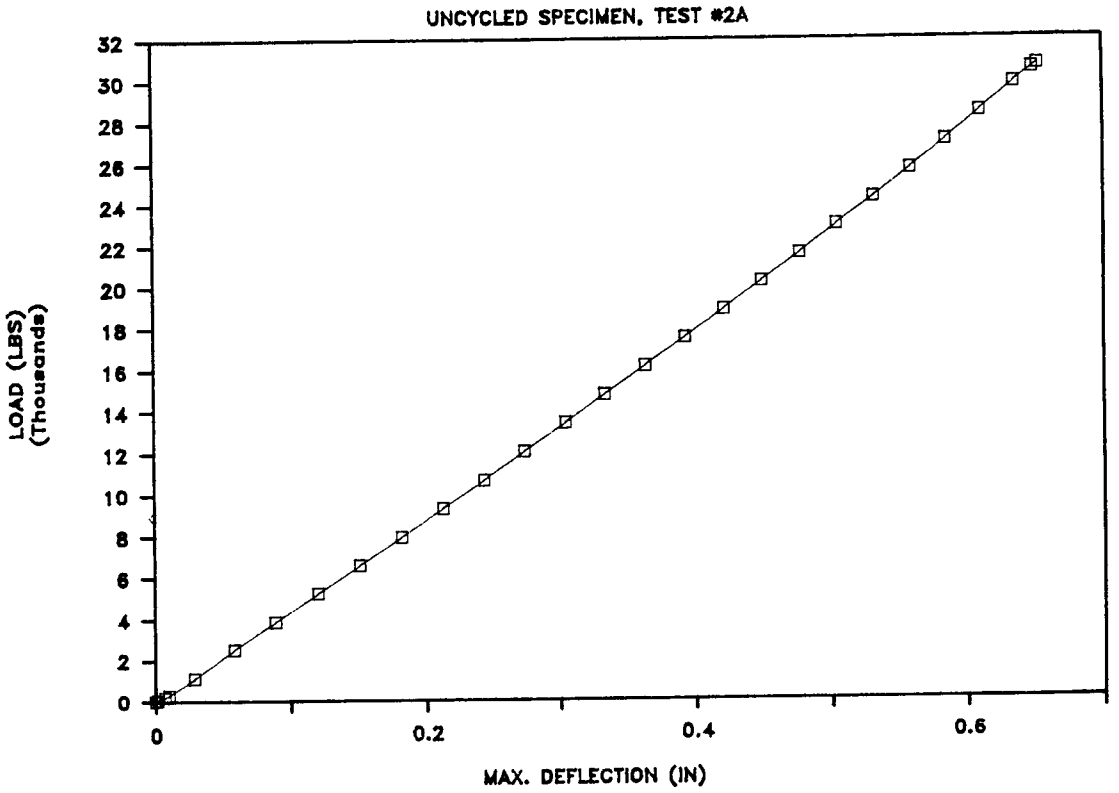

Figure 8. OBR cyclic loads test, uncycled specimen, Test No. 2A.

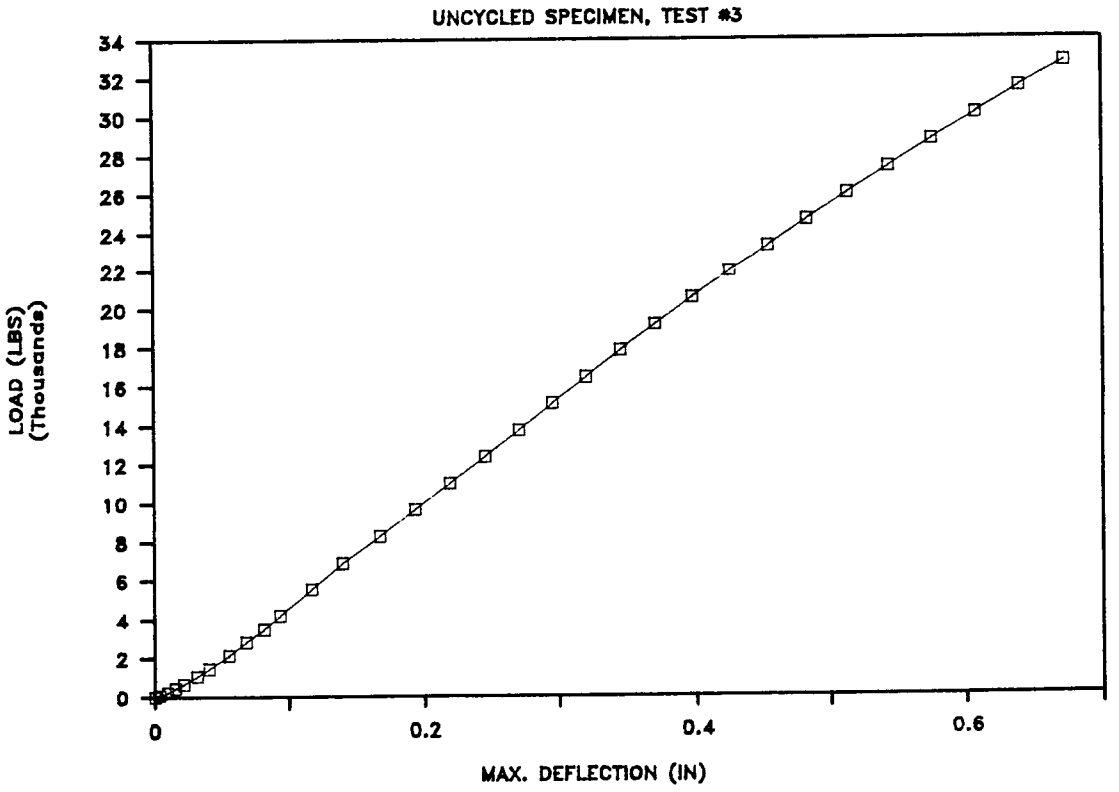

Figure 9. OBR cyclic loads test, uncycled specimen, Test No. 3.

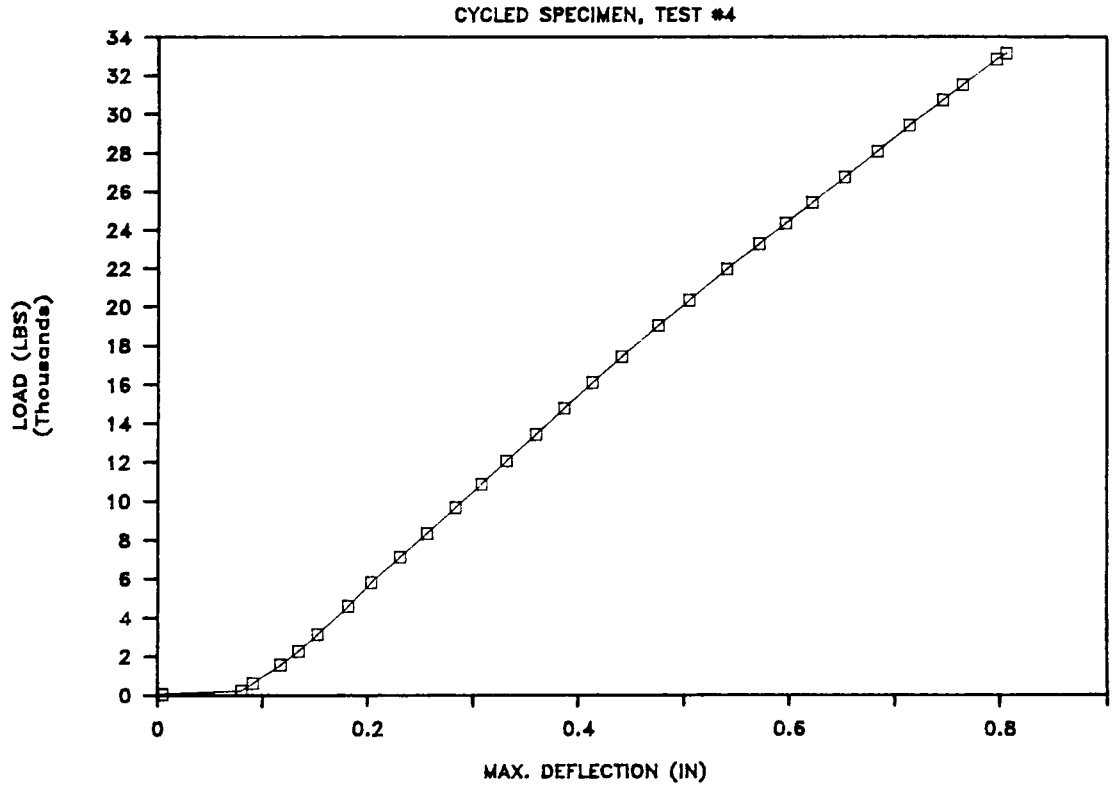

Figure 10. OBR cyclic loads test, uncycled specimen, Test No. 4.

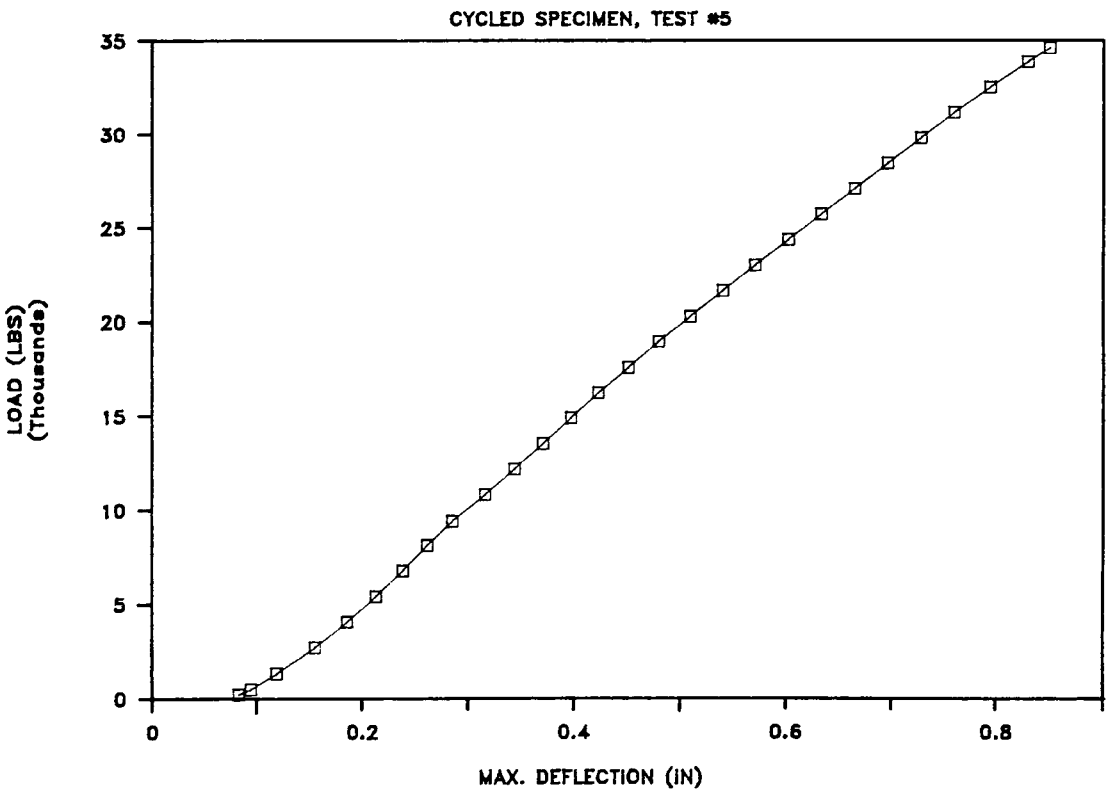

Figure 11. OBR cyclic loads test, cycled specimen, Test No. 5.

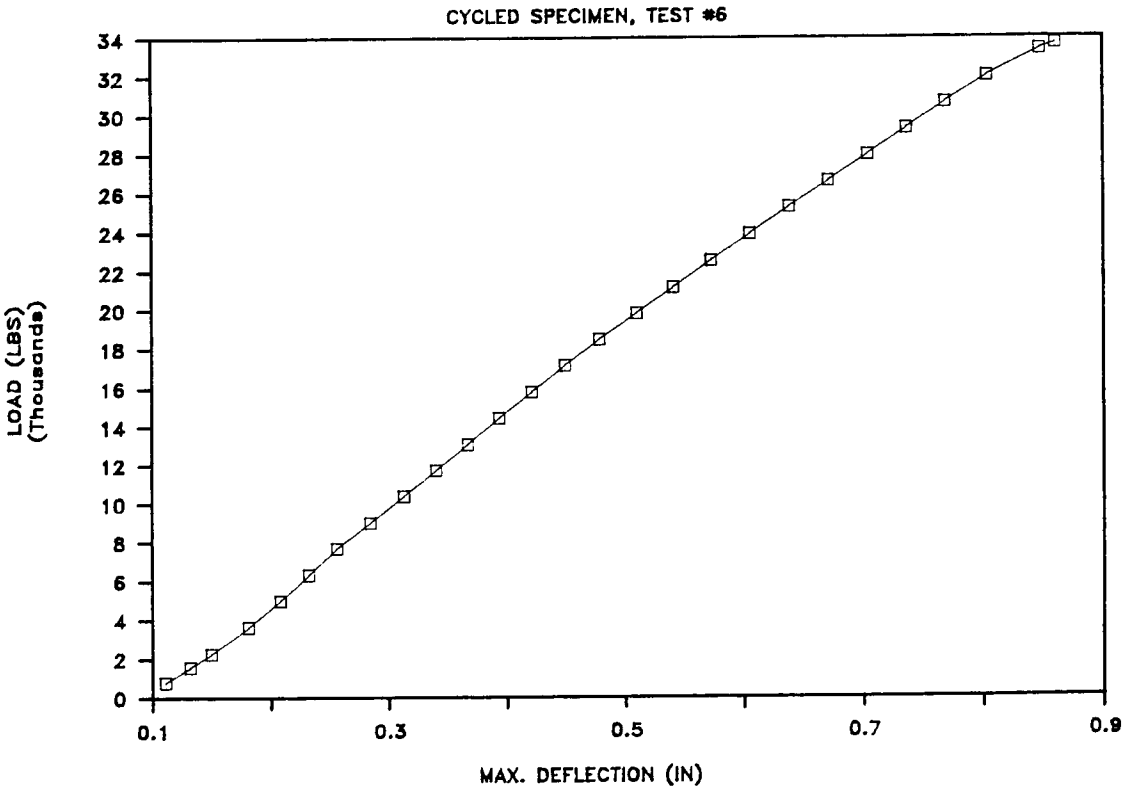

Figure 12. OBR cyclic loads test, cycled specimen, Test No. 6.

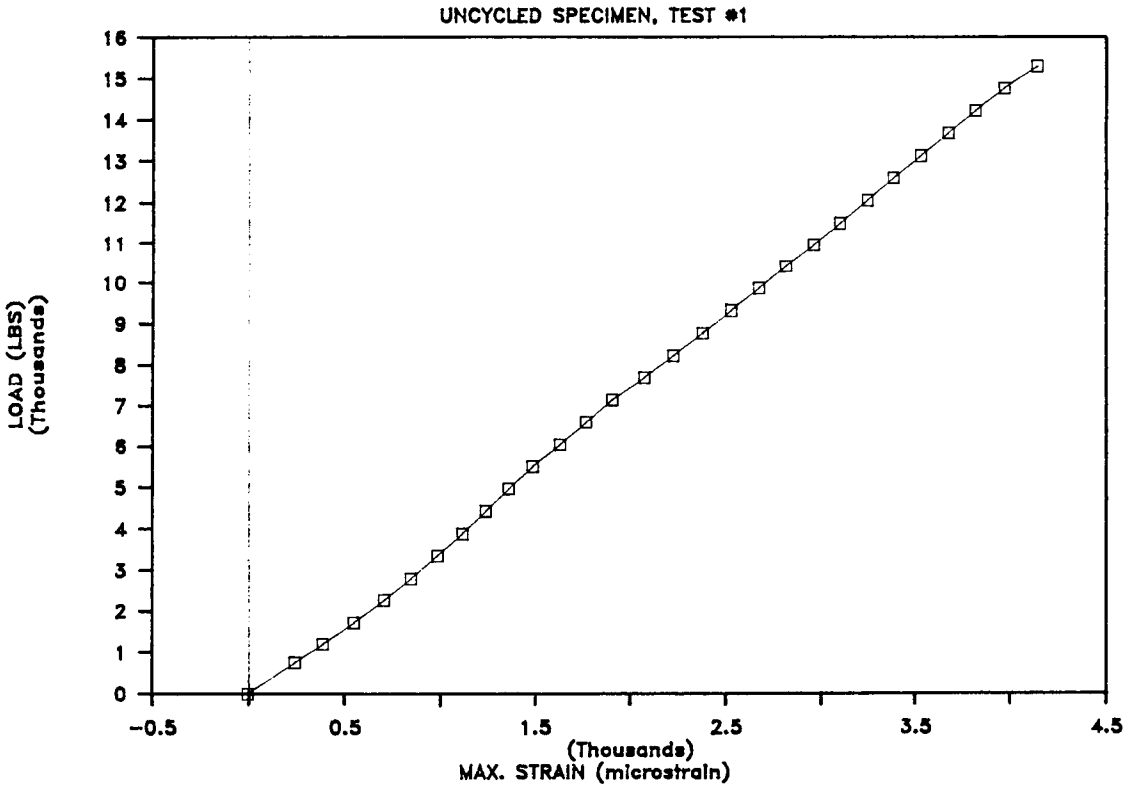

Figure 13. OBR cyclic loads test, uncycled specimen, Test No. 1.

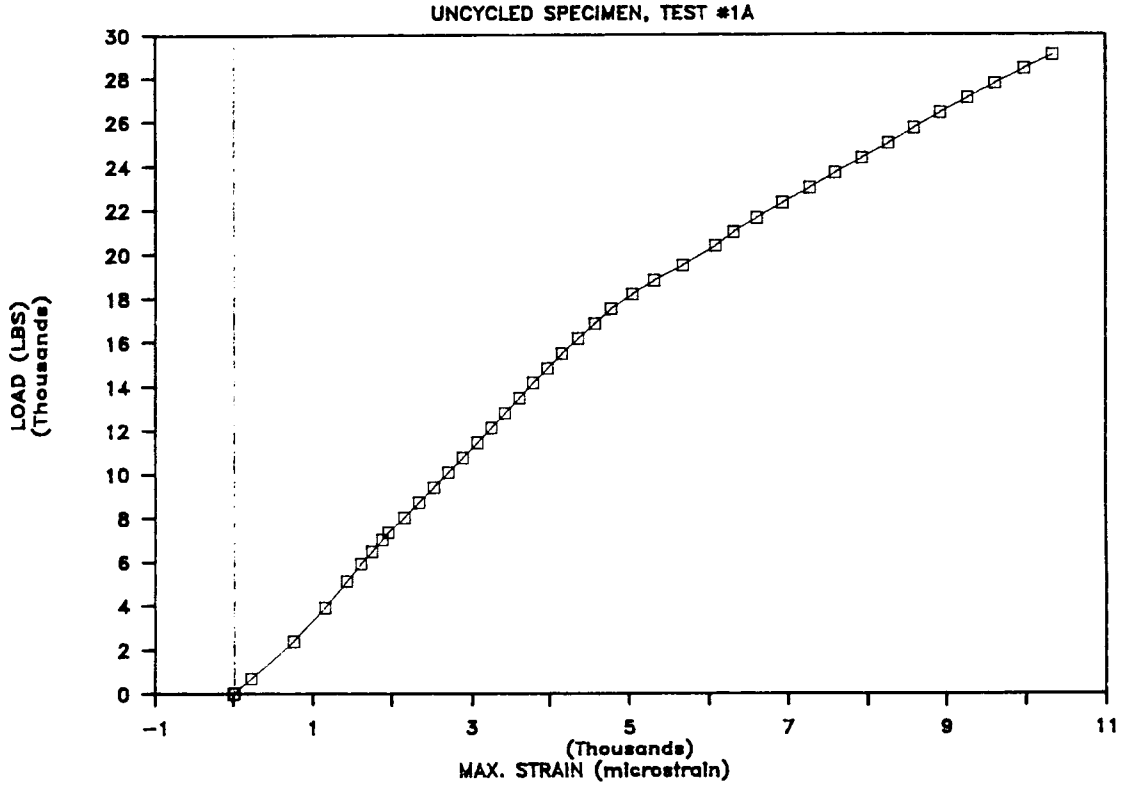

Figure 14. OBR cyclic loads test, uncycled specimen, Test No. 1A.

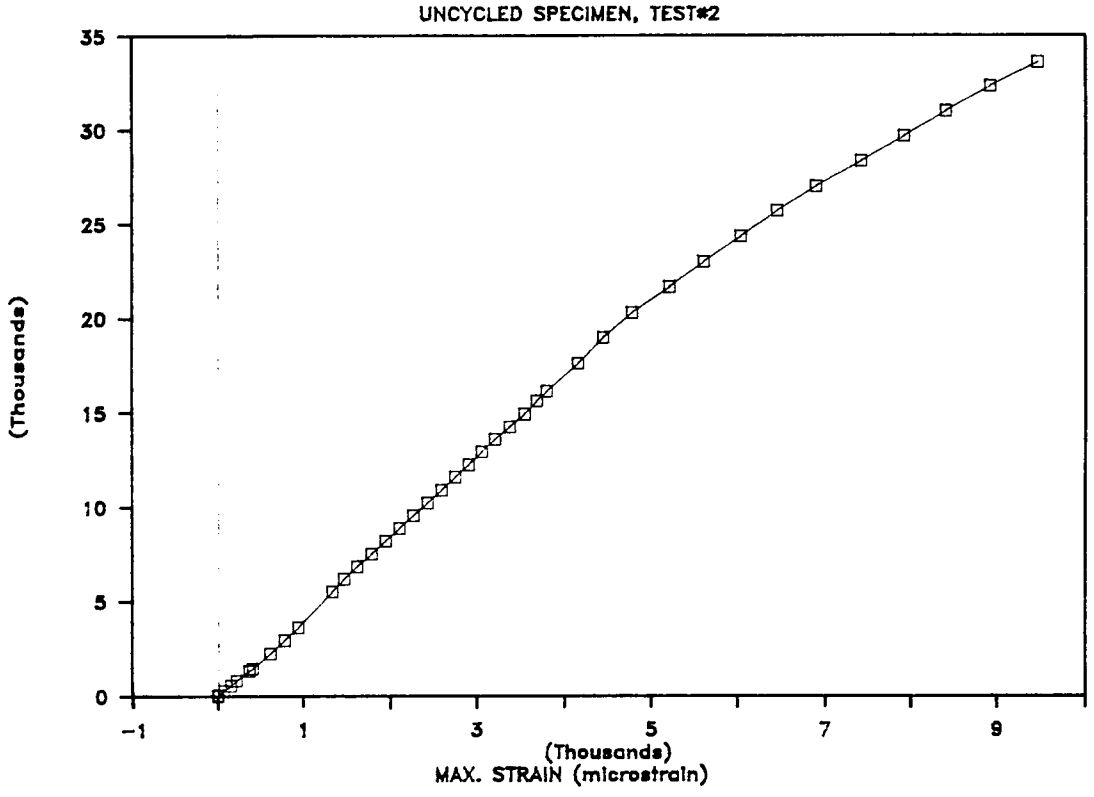

Figure 15. OBR cyclic loads test, uncycled specimen, Test No. 2.

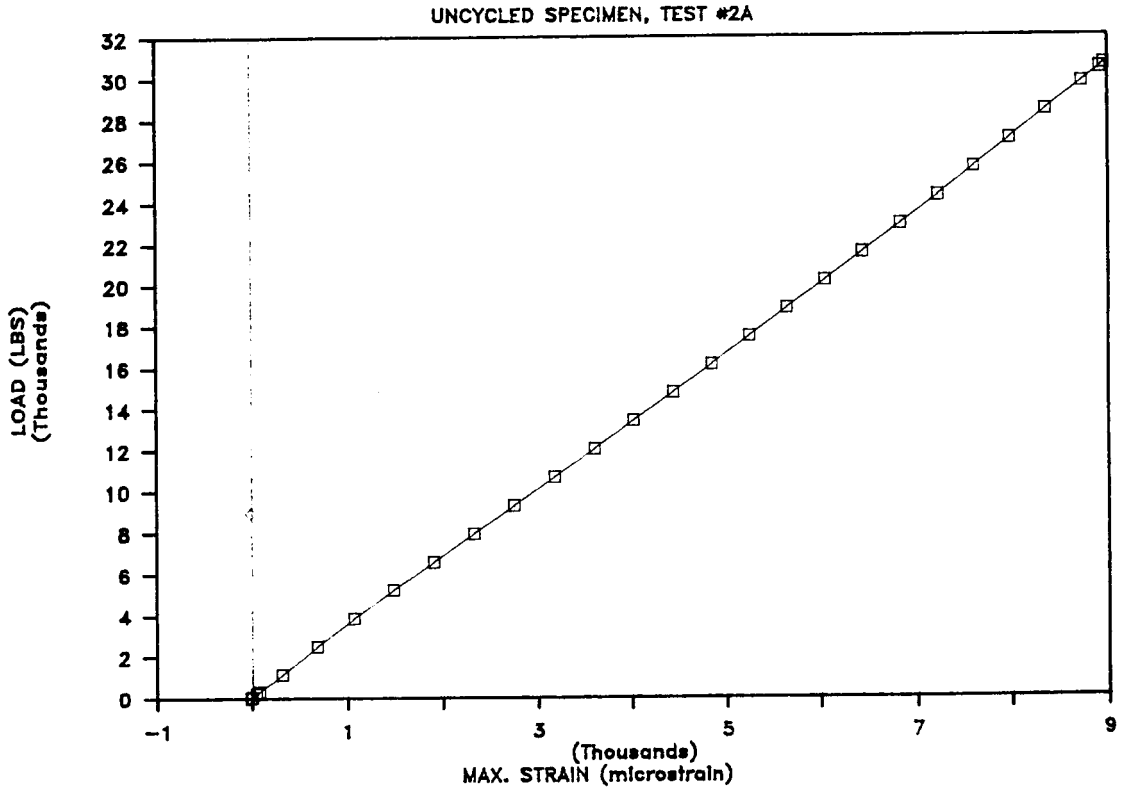

Figure 16. OBR cyclic loads test, uncycled specimen, Test No. 2A.

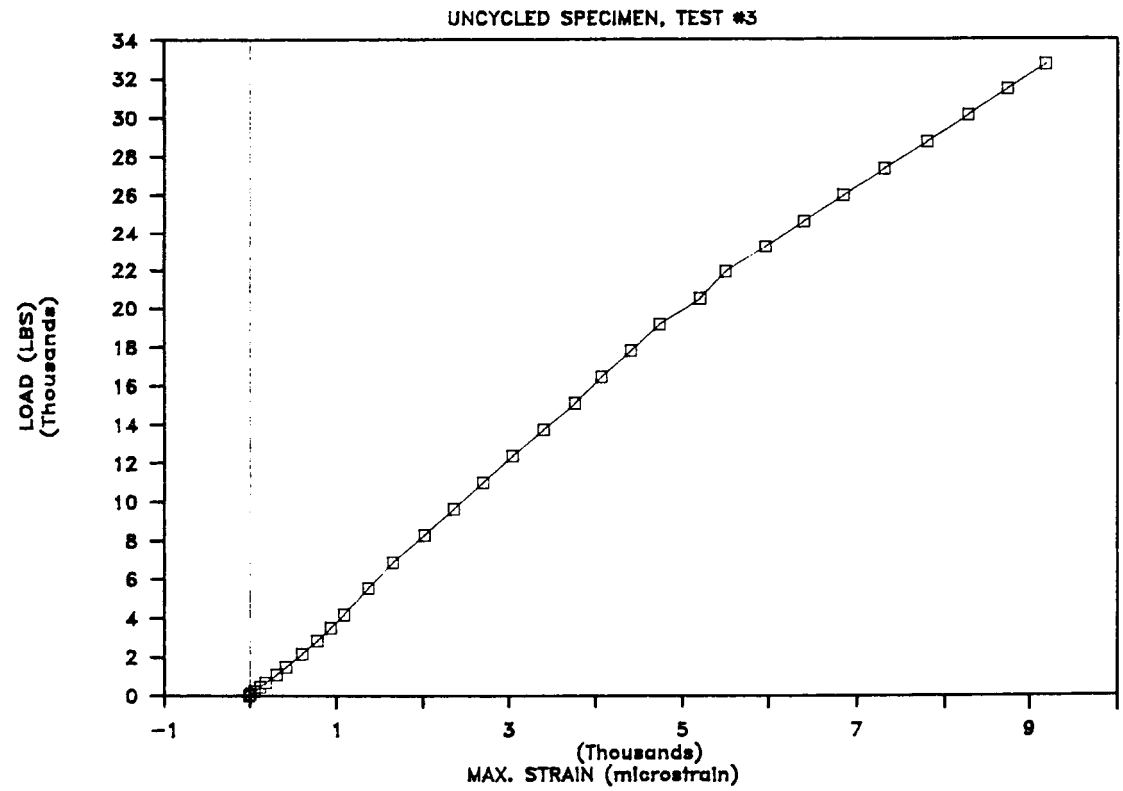

Figure 17. OBR cyclic loads test, uncycled specimen, Test No. 3.

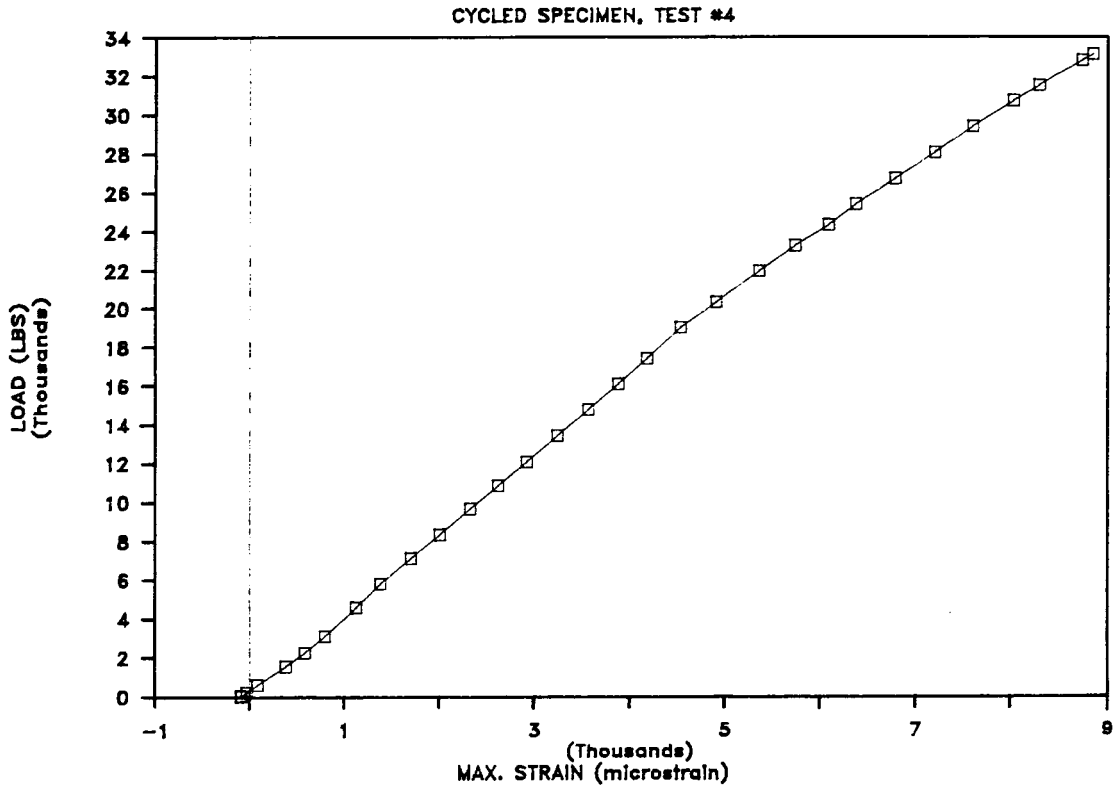

Figure 18. OBR cyclic loads test, cycled specimen, Test No. 4.

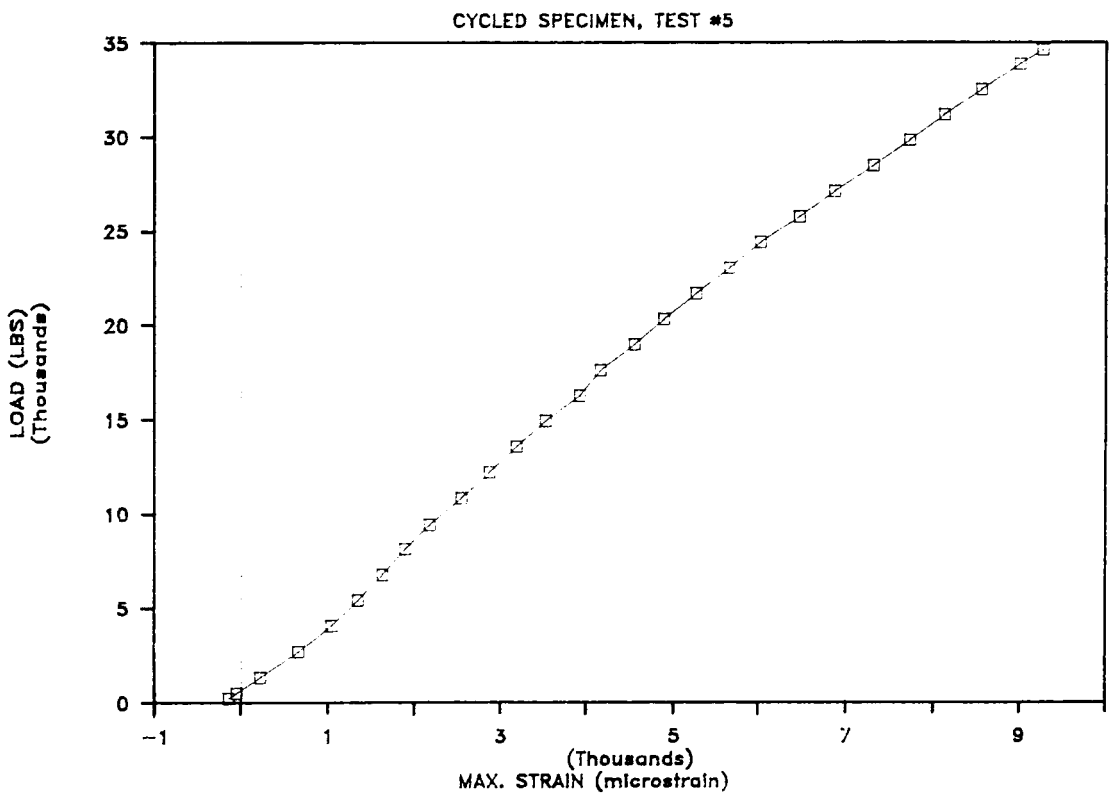

Figure 19. OBR cyclic loads test, cycled specimen, Test No. 5.

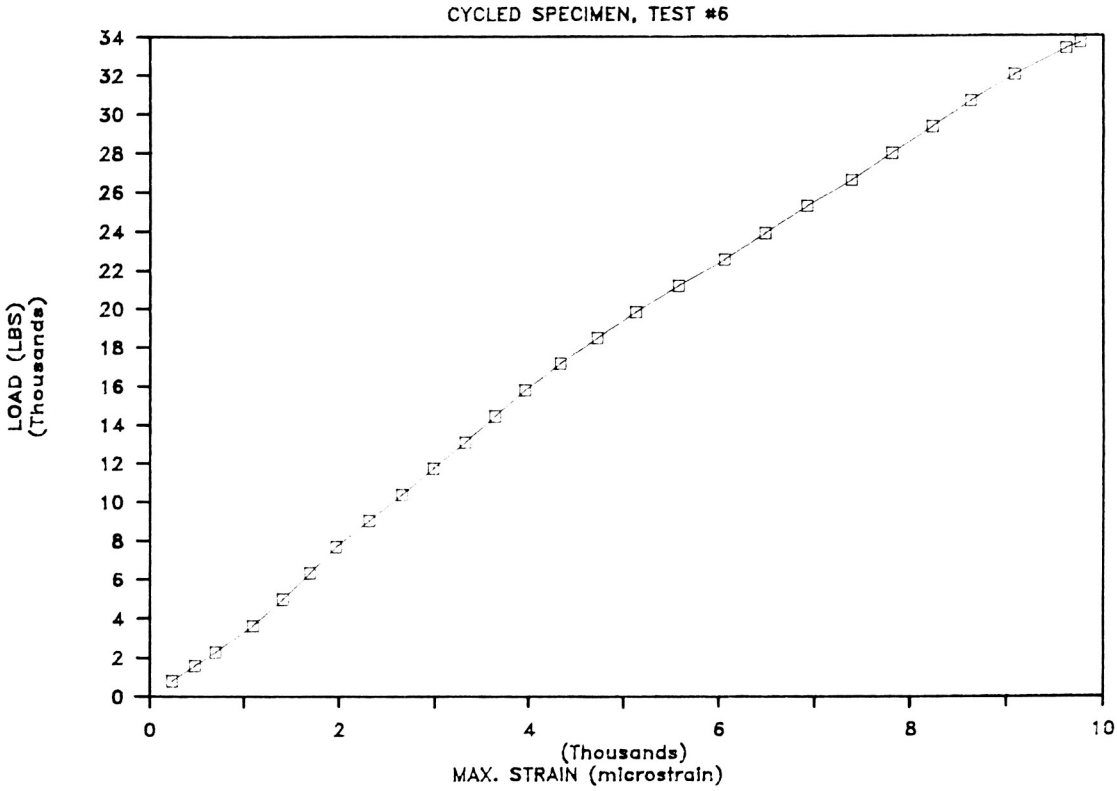

Figure 20. OBR cyclic loads test, cycled specimen, Test No. 6.

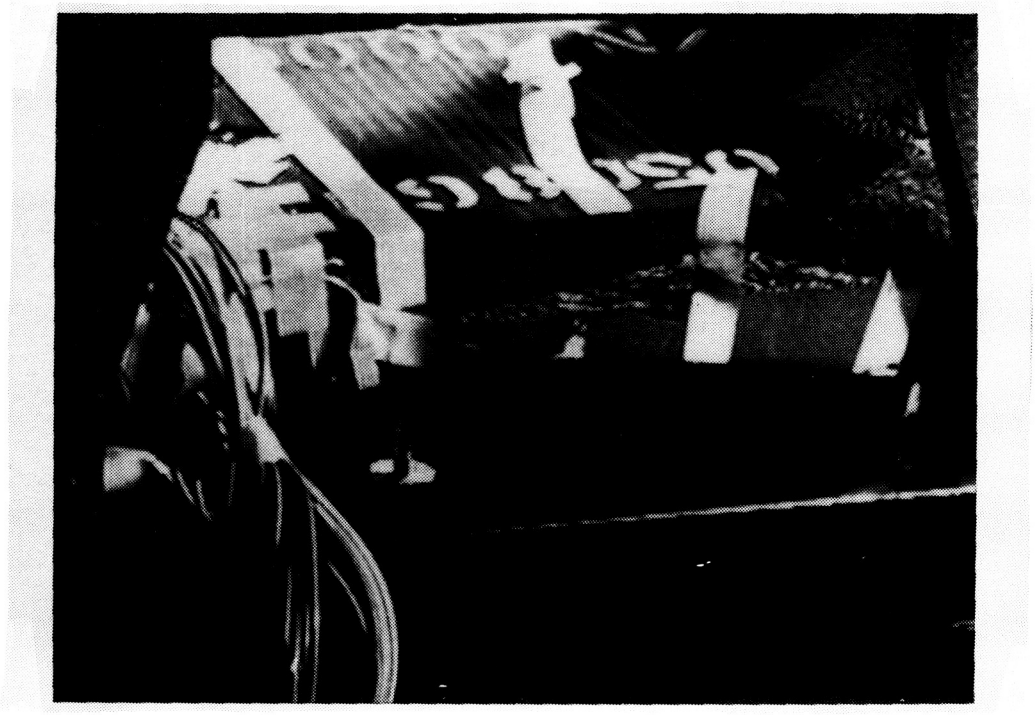

Figure 21. Test setup after failure.

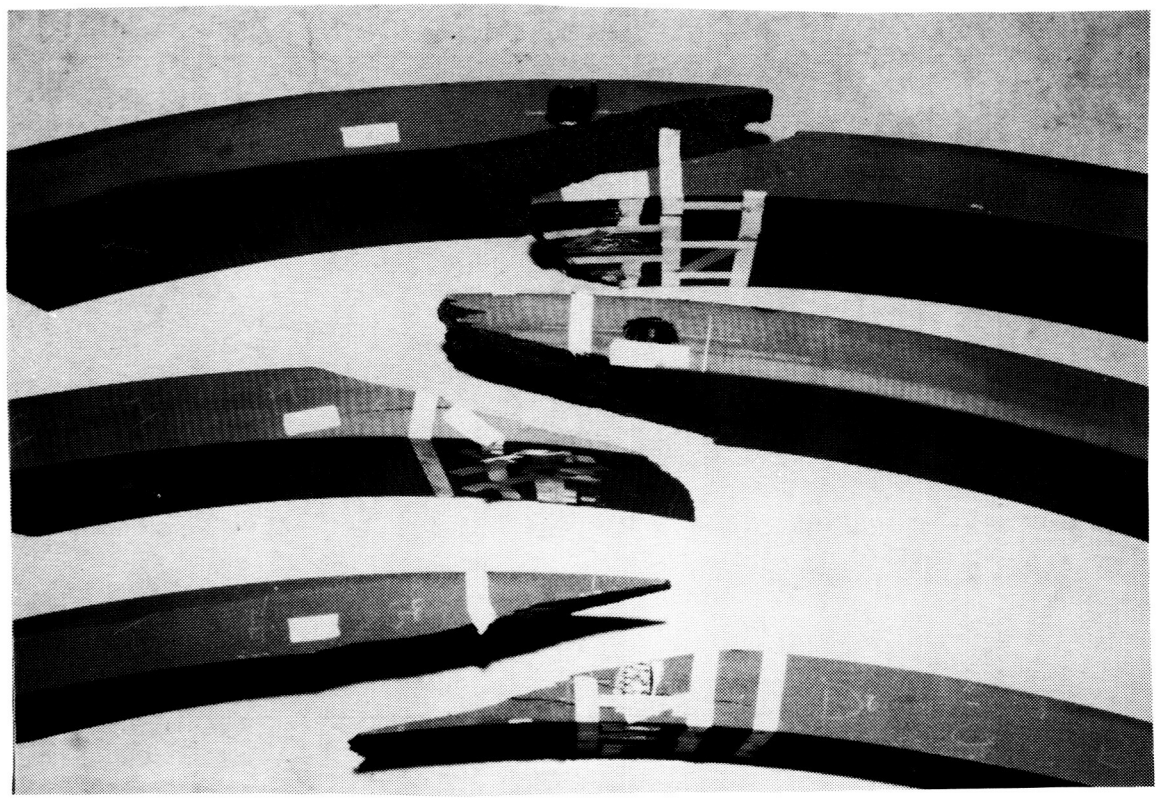

Figure 22. SRB 30-in. segment cyclic load test, uncycled specimens.

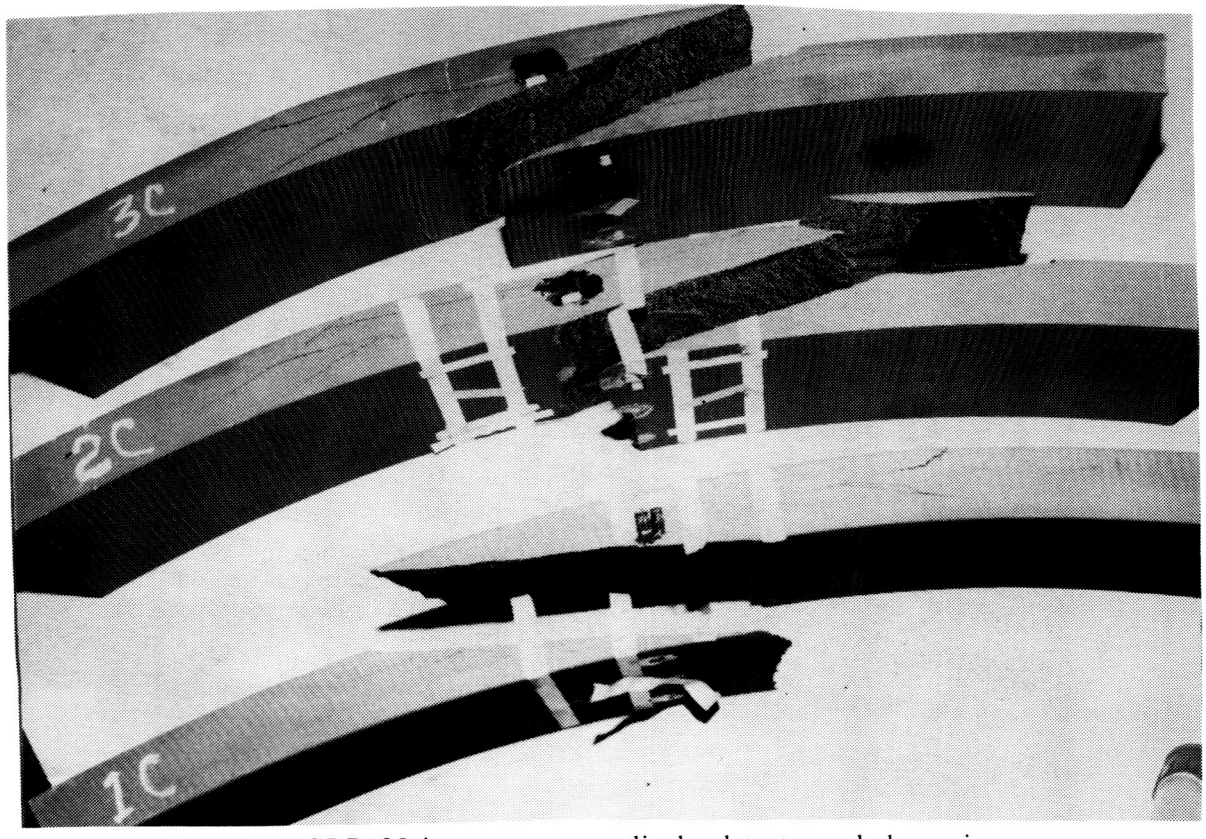

Figure 23. SRB 30-in. segment cyclic load test, cycled specimens.

1. REPORT NO.	2. GOVERNMENT ACCESSION NO.	3. RECIPIENT'S CATALOG NO.
NASA TP-2884		

4. TITLE AND SUBTITLE	5. REPORT DATE
Cyclic Loads Tests of Carbon Involute Solid Rocket Motor Outer Boot Ring Segments	December 1988
	6. PERFORMING ORGANIZATION CODE
7. AUTHOR(S)	8. PERFORMING ORGANIZATION REPORT #
Rafiq Ahmed	
9. PERFORMING ORGANIZATION NAME AND ADDRESS	10. WORK UNIT NO.
George C. Marshall Space Flight Center Marshall Space Flight Center, Alabama 35812	M-605
	11. CONTRACT OR GRANT NO.
	13. TYPE OF REPORT & PERIOD COVERED
12. SPONSORING AGENCY NAME AND ADDRESS	Technical Paper
National Aeronautics and Space Administration Washington, D.C. 20546	14. SPONSORING AGENCY CODE

15. SUPPLEMENTARY NOTES

Prepared by Structures and Dynamics Laboratory, Science and Engineering Directorate.

16. ABSTRACT

This report documents the cyclic loads tests performed on 30-in. segments of the DM-9 configuration Solid Rocket Outer Boot Ring. The tests found that the effect of the cyclic loadings on the structural integrity of the outer boot ring was negligible. The results are compared with a hand analysis of the strength of a 30-in. outer boot ring segment.

Several phenomena of engineering interest are also described in this report.

17. KEY WORDS	18. DISTRIBUTION STATEMENT
Outer Boot Ring Cyclic Loads Tests	Unclassified - Unlimited Subject Category 39

19. SECURITY CLASSIF. (of this report)	20. SECURITY CLASSIF. (of this page)	21. NO. OF PAGES	22. PRICE
Unclassified	Unclassified	29	A02

For sale by National Technical Information Service, Springfield, Virginia 22161

NASA-Langley, 1988